The Range Safety Debris Catalog Analysis in Preparation for the Pad Abort One Flight Test

Prasad M. Kutty*
Analytical Mechanics Associates, Inc., NASA Dryden Flight Research Center, Edwards, California, 93523

William D. Pratt†
Lockheed Martin Space Systems Company, Denver, Colorado 80201

The Pad Abort One flight test of the Orion Abort Flight Test Program is currently under development with the goal of demonstrating the capability of the Launch Abort System. In the event of a launch failure, this system will propel the Crew Exploration Vehicle to safety. An essential component of this flight test is range safety, which ensures the security of range assets and personnel. A debris catalog analysis was done as part of a range safety data package delivered to the White Sands Missile Range in New Mexico where the test will be conducted. The analysis discusses the consequences of an overpressurization of the Abort Motor. The resulting structural failure was assumed to create a debris field of vehicle fragments that could potentially pose a hazard to the range. A statistical model was used to assemble the debris catalog of potential propellant fragments. Then, a thermodynamic, energy balance model was applied to the system in order to determine the imparted velocity to these propellant fragments. This analysis was conducted at four points along the flight trajectory to better understand the failure consequences over the entire flight. The methods used to perform this analysis are outlined in detail and the corresponding results are presented and discussed.

Nomenclature

ACM	=	Attitude Control Motor
AFT	=	Abort Flight Test
AM	=	Abort Motor
a	=	acceleration, ft/s^2
C	=	number of groups in class c
CAS	=	cylindrical annular sector
CEV	=	Crew Exploration Vehicle
CM	=	Crew Module
C_v	=	specific heat at constant volume, ft-lb/slug-k
c	=	speed of sound, ft/s
c_d	=	drag coefficient
$c_{discharge}$	=	discharge coefficient of the chamber
d	=	step width between standard deviations (0.01 for 601 steps)
E	=	energy, ft-lb
$\dot{E}$	=	energy flow rate, ft-lb/s
F	=	force, lbf/ft
FTA	=	Flight Test Article
H	=	scaling factor
h	=	enthalpy, ft-lb/slug
h_0	=	longest cross sectional half width of the fragment, ft
JM	=	Jettison Motor

* Aerospace Engineer, Controls & Dynamics Branch, P.O. Box 273/MS 4830E, AIAA Member.
† Mission Analyst, Human Space Flight, P.O. Box 179/MS W3003.

k = weight group index
LAS = Launch Abort System
LAV = Launch Abort Vehicle
M = mass, lbm
M_l = mass per unit length, lbm/ft
$\dot{M}$ = mass flow rate
m = midpoint step number (301 for 601 steps)
N = total number of weight groups
NASA = National Aeronautics and Space Administration
n = frequency of fragment
P = pressure,psf
PA-1 = Pad Abort One
R = ratio of pressures between control volumes
RSRM = Reusable Solid Rocket Motor
r = radius, ft
S = area per unit length, ft
SepRing = Separation Ring
SM = Service Module
s = standard deviation of group distribution
T = temperature, Kelvin
V = volume per unit length, ft^2
v = velocity, ft/s
$\dot{W}$ = energy flow rate due to work done by control volume, ft-lb/s
WSMR = White Sands Missile Range
w = weight of fragment, lbm
X = variable described by probability density function
x = position, ft
Y = probability density function
y = group index number of the first group in class c
z = group index number of the last group in class c
β = ballistic coefficient, lb/in^2
γ = ratio of specific heats of the combustion gases
Δt = time step, s
Δv = change in velocity over corresponding time step, ft/s
Δx = change in position over corresponding time step, ft
μ = mean of probability density function
ρ = density, $slug/ft^3$
σ = standard deviation of probability density function
τ = fragment thickness, ft

Subscripts
c = fragment class index
crack = crack width
flow, in = flow into control volume
flow, out = flow out of control volume
frag = fragment
i = time step index
j = control volume index
k = fragment group index
L = largest fragment group
S = smallest fragment group
1 = chamber control volume
2 = propellant-case gap control volume
3 = atmosphere control volume

I. Introduction

The Orion Abort Flight Test (AFT) Program is an essential component of the Constellation Program architecture. Its objective is to develop and validate the Launch Abort System (LAS) as a reliable escape vehicle for reducing astronaut risk during Constellation missions. Flight testing of this system is scheduled to begin in early 2010. With each flight test, a comprehensive range safety analysis package will be provided to the test range describing the functionality of the LAS as well as specific failure mode studies requested by the test range. This paper presents an analysis included in that package; the debris catalog analysis for the first flight test, Pad Abort One (PA-1).

A PA-1 debris catalog analysis was completed and submitted to the range describing the consequences of an overpressurization failure of the solid rocket Abort Motor (AM) during the test. Specifically, the analysis was done to characterize the propellant debris distribution as a result of such a failure. This characterization was done using a statistical model to estimate potential propellant debris sizes, shapes, and frequencies. Additionally, ejection velocities for each propellant debris fragment were computed. The velocities were calculated using an iterative energy balance method to converge upon a solution. The debris catalog analysis was parametrically performed by evaluating the debris distribution and ejection velocities at four stages on the AM profile. It was shown that consistent trends exist describing the distribution as a function of AM propellant remaining and the velocity as a function of fragment size.

It should be noted that the methods used in this report are expanded upon from other sources[1] and applied to PA-1. These sources describe a method of debris catalog analysis used for solid rocket motors larger than the AM being considered. For the purposes of this analysis, it is assumed that the methodology is still valid as applied to the AM.

II. Constellation and PA-1 Overview

As the National Aeronautics and Space Administration (NASA) begins to bring the Space Shuttle Program to an end, work is underway on the Shuttle's successor, the Constellation Program. Constellation marks a new phase in the manned space program of the United States, relying upon design influences from both the Apollo and Space Shuttle programs while utilizing more modern technology. The Constellation architecture employs a cargo launch vehicle, the Ares V; and a crew launch vehicle, the Ares I (shown in Fig. 1). More information on Constellation architecture and concept of operations can be found in Ref. 2. Residing on top of the Ares I booster is the Orion Vehicle, shown in the left portion of Fig. 1. Orion is the crewed section of Constellation, consisting of the LAS, the Crew Module (CM), the Service Module (SM), and the separation ring (SepRing). Together, the LAS and CM are referred to as the Launch Abort Vehicle (LAV). The LAS is a component of Orion designed to ensure crew safety; it is to be used as an egress vehicle should the crew need to escape from the Ares I rocket. Being the last line of safety for the astronauts in the event of an emergency, the LAS must be particularly reliable. As such, Orion will take advantage of flight testing to produce an operational LAS. These tests are part of the Orion Crew Exploration Vehicle (CEV) AFT Program managed by NASA's Dryden Flight Research Center; an essential component of the Constellation architecture dedicated to flight testing the LAV. More information on the AFT Program can be found in Ref 3.

The first of these flight tests, Pad Abort One (PA-1), aims to simulate an abort from the launch pad and is scheduled to take place in early 2010 at the White Sands Missile Range (WSMR) in New Mexico. The Flight Test Article (FTA) configuration is shown in Fig. 2, and excludes both the Service Module (SM) and the Ares I booster. The largest and most powerful motor on the LAS is the AM, which is specifically designed to pull the CM off of the Ares I. PA-1's primary objective is to demonstrate the ability of the LAS to propel the CM away from the launch vehicle during a pad abort scenario. Other test objectives include verification of control, stability, and performance characteristics of the LAV. More information on PA-1 can be found in Ref. 4.

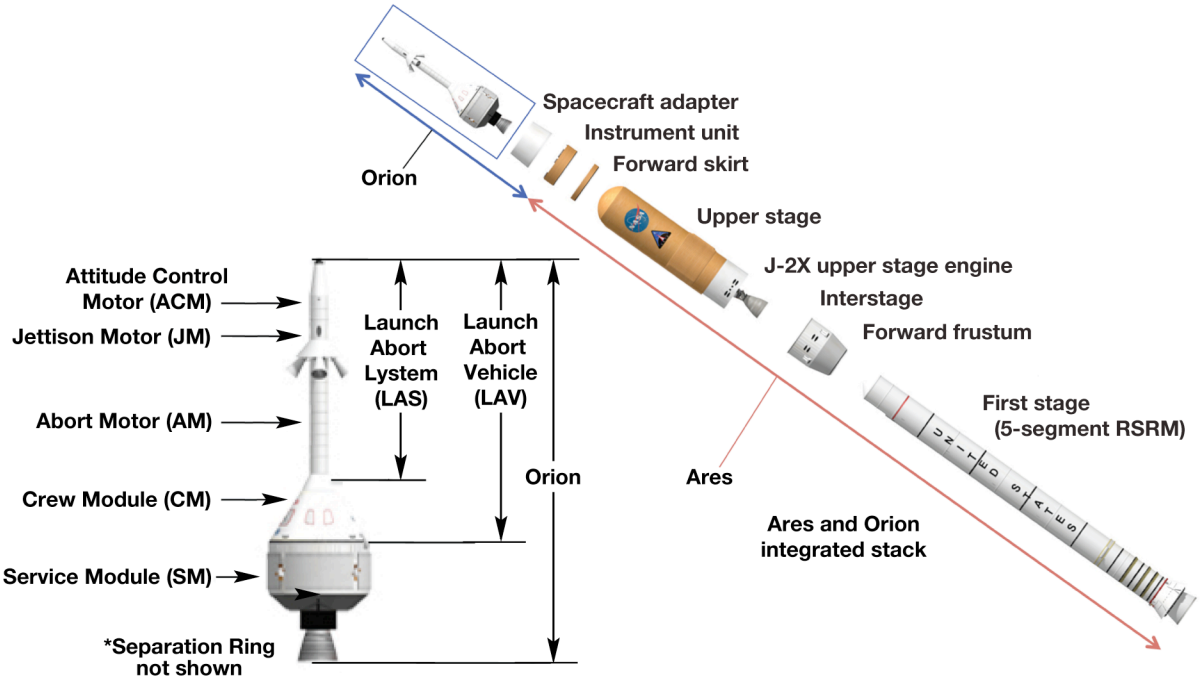

Figure 1. Description of Orion and Ares I Launch Vehicle.

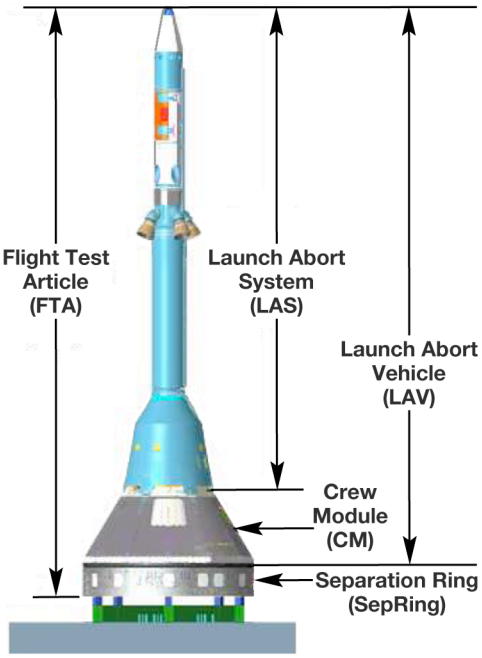

Figure 2. PA-1 vehicle configuration.

While these objectives promote technological development for future Constellation missions, range safety during the test must be assured. For PA-1, as with each flight test, a range safety analysis is provided to the WSMR Safety Office to understand the potential consequences of various failure scenarios during the mission. This data package consists of physical and functional descriptions of the vehicle, flight event sequence, performance and trajectory information, and vehicle failure modes. One of these analyses is a debris catalog study for an in-flight breakup of the LAS. The goal of this analysis is to characterize the debris generated during this failure mode and its hazard to the

range. The definition of a debris catalog is given in Section III, "Debris Catalog Task Overview," along with the specific analysis required for PA-1.

This report will present the methodology and results of the debris catalog analysis for PA-1. A discussion of the results, as well as limitations and assumptions carried by the analysis will be provided.

III. Debris Catalog Task Overview

In general, a debris catalog analysis can be defined as a prediction of frequency, size, and velocity of debris fragments created in the explosion of a launch vehicle. This data is used by range safety engineers to determine the potential hazard posed by a launch failure for a particular mission. For PA-1, this type of analysis was requested by the WSMR Safety Office to understand the consequences of an AM failure during the test. Specifically, the task objective seeks weight, shape, and area specifications for debris fragments as well as corresponding ballistic coefficients and ejection velocities. As described in this report, area refers to cross-sectional fragment area, and ejection velocity refers to the relative velocity between the fragment and the vehicle as the fragment departs the vehicle. Also, frequency refers to the number of fragments for a particular fragment weight.

The PA-1 analysis considers a failure scenario in which the Abort Motor (AM) of the vehicle overpressurizes beyond the ultimate strength of the case. Possible causes for such a scenario include a plugged nozzle, cracks in the propellant grain, or other flaws that could cause an extreme build up of pressure in the motor chamber. As a result of the excessive internal pressures in the motor chamber, this analysis assumes a case rupture generating a debris field composed of propellant and structural fragments. Although an AM failure could result in other failure modes, several of which were provided to the range, the debris field mode is studied here. With a maximum thrust of roughly 500,000 lbf and a maximum operating pressure of 1,750 psi, an AM failure is assumed to result in the most energetic debris compared against failures of other motors onboard PA-1. This assumption bounds the problem as a worst-case condition. Another consideration worth noting is the grain geometry of the AM. While the actual PA-1 AM grain geometry is a wagon wheel design[5] (shown in Fig. 3), it is simplified to a cylindrical design for this analysis.

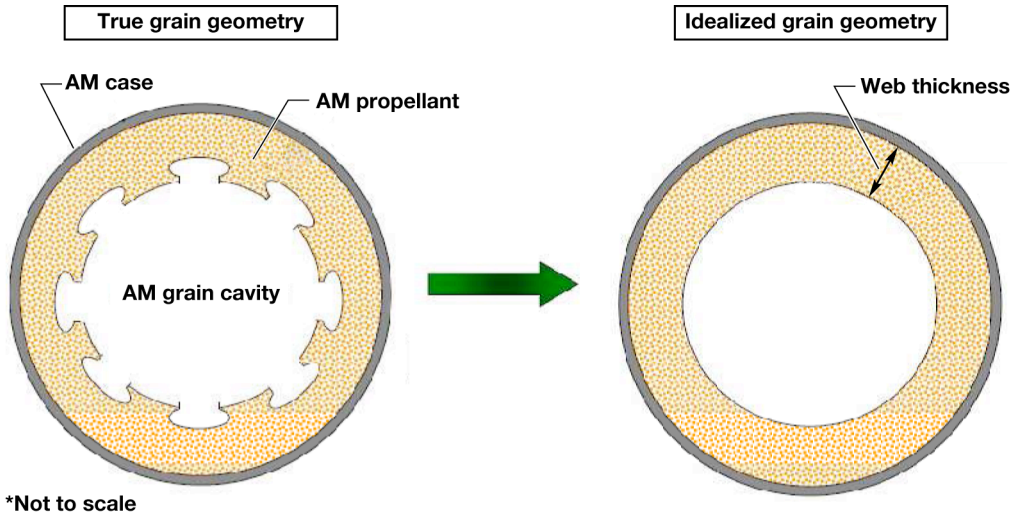

Figure 3. Comparison of actual and idealized grain geometries.

The solution to this problem can be divided into three different steps[1]. The first step, described in Section IV, "Debris Catalog Distribution," is the modeling of the propellant breakup distribution using trends determined by observation of similar failures. This model provides a catalog of fragments specifying weight, size, shape, and frequency for all debris potentially generated in the motor blast. The second step, described in Section IV.C, "Ballistic Coefficient Computation," is the determination of ballistic coefficients for each debris item. The third step, described in Section V, "Fragment Ejection Velocities," is the calculation of imparted velocities for each debris item using a method of imparting the energy contained in the motor to the various fragments contained in the debris catalog. Using these three steps, a debris catalog was assembled for the range to identify the safety implications of an AM overpressure failure during PA-1.

The PA-1 trajectory is used in this analysis by providing the reference flight conditions about which potential in-flight breakups must be analyzed. A nominal reference trajectory designed by the PA-1 Flight Dynamics Team was used. From the trajectory, a point in flight must be chosen to analyze the overpressure failure. To bound the impact of this assumption on results, the study was performed parametrically. The assumed failure points, referred to as 'burn stages,' represent the amount of propellant spent at the time of failure (i.e. 25% burn stage = 25% propellant burned or 75% propellant remaining). Because vehicle flight conditions such as Mach number, altitude, and heading are functions of time, their values at each burn stage are an important input to the analysis. With that in mind, four burn stages were chosen to estimate a debris catalog at various points along the trajectory: 0% (on the pad), 25%, 50%, and 75%. These were selected under the assumption that the amount of propellant remaining would drive the trends seen in the results because the remaining propellant would determine the amount of mass available for the debris distribution. Four evenly spaced stages along the AM propellant mass profile would then sufficiently capture the debris catalog characteristics over the life of the AM. Note that the AM propellant is completely spent after only seven seconds of flight and although the entire test endures over eighty seconds, these first seven are crucial to this task.

IV. Debris Catalog Distribution

The distribution model, a log-normal statistical model is described in Section IV.A, "Model Selection: Log-Normal Distribution." In this section, the statistical approach is explained including the motivation for using such a model. Section IV.B, "Model Selection: Log-Normal Distribution," provides the statistical tools required to apply the model to a solid rocket motor to obtain a propellant fragment distribution. A theoretical example is given for the reader to better understand how the method is applied. Section IV.C, "Ballistic Coefficient Computation," discusses the computation of area and ballistic coefficient.

A. Model Selection: Log-Normal Distribution

The first step in completing the PA-1 debris catalog was to characterize the debris field resulting from an explosion of the Abort Motor to include fragment geometries, weights, and frequencies. This characterization was accomplished using a statistical estimation model, precluding the need for a high fidelity structural breakup model. Previous research involving booster failures have revealed consistent breakup patterns that can be modeled statistically and applied towards large solid rocket motors.[1] These investigations used video footage of launch vehicle failures, such as the Titan 34D (Martin Marietta Corporation now Lockheed Martin, Bethesda, Maryland) in 1986, to make observations of the size and frequency of fragments produced during such accidents.[1] The visual observations yield statistical trends among the resulting debris fragments that have been applied to other solid boosters such as the Space Shuttle's solid rocket boosters.[6] This statistical approach is an accepted method of characterizing debris distributions for solid rocket failures.

This model relies on a log-normal statistical distribution to capture debris characteristics. A log-normal distribution describes a relationship between a variable and its logarithm. By definition, the logarithm of a log-normally distributed variable is normally distributed.[7] Eq. (1)[7] is a general equation for a log-normal distribution. In this equation, X is the variable being distributed, Y is the probability density function of X, σ is the standard deviation of the distribution, and μ is the mean of the distribution.

$$Y = \left(\frac{1}{X\sigma\sqrt{2\pi}} \right) \times \exp\left(-\frac{(\ln X - \mu)^2}{2\sigma^2} \right) \tag{1}$$

Shown in Fig. 4, the bulk of log-normally distributed data is biased towards the front end of its distribution as opposed to its center or mean as is the case with a normal distribution. Applied to a debris catalog analysis, this log-normal distribution describes a solid rocket debris model as having a higher frequency of smaller fragments and a logarithmic decay in frequency as fragment size increases. Note that this statistical model is applied only to the propellant fragments generated by the motor malfunction. The breakup behavior of the motor case was not expected to follow a log-normal distribution because of its composite material. Therefore, this report deals with the debris catalog characteristics of only the AM propellant.

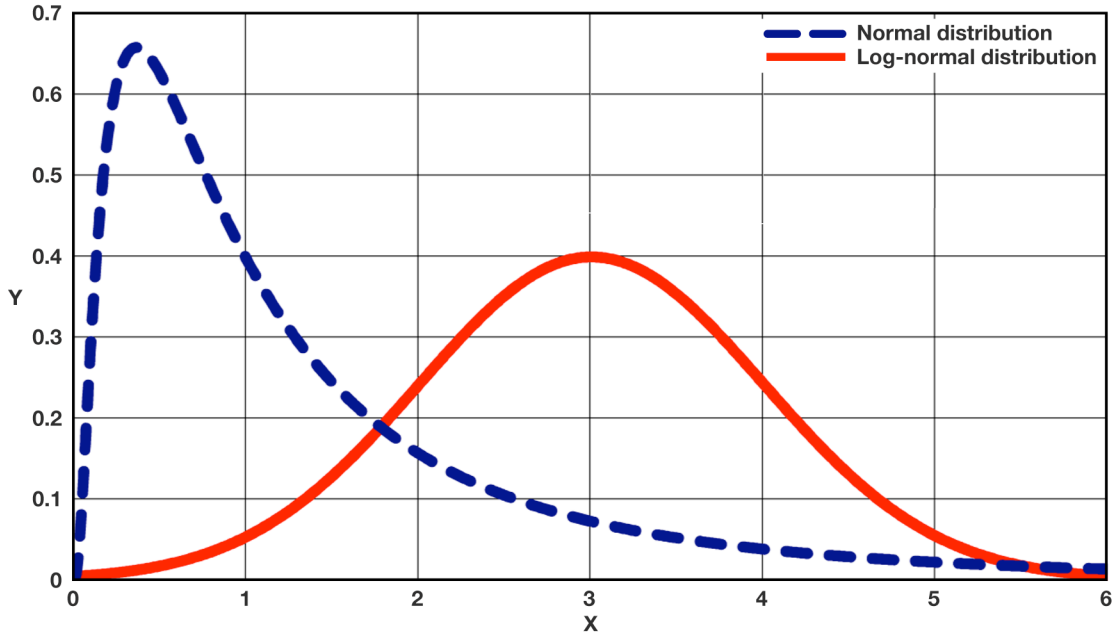

Figure 4. Comparison of log-normal and normal statistical distribution.

B. Model Application: PA-1 Debris Catalog Distribution

Employing the above method yields a propellant debris field distribution for the solid rocket Abort Motor used on the LAS. The distribution was discretized into 601 weight groups that were normally distributed with respect to the logarithms of their weights.[1] Each weight group represents 0.01 standard deviations of the distribution: group 1 represents -3 standard deviations, group 601 represents +3 standard deviations, and all other groups linearly correspond to the standard deviations between -3 and +3 (i.e. group 2 is -2.99 standard deviations, group 600 is +2.99 standard deviations, etc.). Weight group values were calculated through a function of natural logarithms of the smallest and largest fragment weights, described by Eq. (2),[1] where k is the weight group index, w_k is the weight value, w_s is the smallest weight in the group distribution, w_L is the largest weight in the group distribution, and N is the number of groups being used, 601 in this study.

$$w_k = \exp\left(\ln w_s + \frac{(k-1)(\ln w_L - \ln w_s)}{N-1} \right) \tag{2}$$

Note that the distributions in this report are referred to in terms of weight (i.e. weight groups and classes) to be consistent with the reference material,[1] but it was convenient in this analysis to use mass values. It is practical to use either property, as long as it is clearly and consistently used. Mass will be used in this paper to describe the fragment debris catalog.

In Eq. (2), the value for w_L was chosen as one percent of the total propellant mass at that stage, consistent with previous analyses.[1] The value of w_s was fixed at 0.2 lbm, which was determined to be an appropriate lower bound on fragment mass. Next, the number of fragments per group can be described by a normal distribution, shown in Eq. (3),[1] where n_k is the weight frequency, H is a scaling factor, d (0.01 for 601 groups) is the step width between standard deviations, and s is the standard deviation.

$$n_k = H \times d \times \frac{1}{\sqrt{2\pi}} e^{\frac{1}{2}s^2} \tag{3}$$

In Eq. (3), the variable H is iteratively determined so that the cumulative weight of all weight groups sums to the propellant remaining at the chosen burn stage. The variable s in Eq. (2) is the standard deviation of the distribution and can be calculated using Eq. (4), where m is the midpoint group number.

$$s = d(k - m) \tag{4}$$

For further clarification of the technique described above, a simple theoretical example will be given. In this example, a log-normal distribution will be applied to a solid rocket motor with a propellant mass of 1,000 lbm at the time of destruct. Table 1 shows how Eqs. (2) to (4) are utilized to assemble the group distribution of this motor. Note that, w_L and w_s, are constant values at each burn stage, corresponding to the largest and smallest weight groups in the group distribution, 10.0 lbm and 0.2 lbm, in Table 1. In looking at the data, two behaviors are noteworthy: (1) the group weights increase exponentially, and (2) group frequency is distributed normally. These behaviors are consistent with the equations that describe them, Eqs. (2) and (3); and are consistent with the definition of a log-normal distribution, a normal distribution of the logarithm of a variable. Figure 5 shows these behaviors graphically.

Table 1. Example of group distribution for propellant fragments.

k	s	w_k(lbm)	n_k
1	-3.00	0.200	0.0256
2	-2.99	0.201	0.0264
3	-2.98	0.203	0.0272
4	-2.97	0.205	0.0280
5	-2.96	0.207	0.0288
…	…	…	…
301	0	1.414	2.303
…	…	…	…
597	+2.96	9.743	0.288
598	+2.97	9.806	0.280
599	+2.98	9.870	0.0272
600	+2.99	9.350	0.0264
601	+3.00	10.000	0.0256

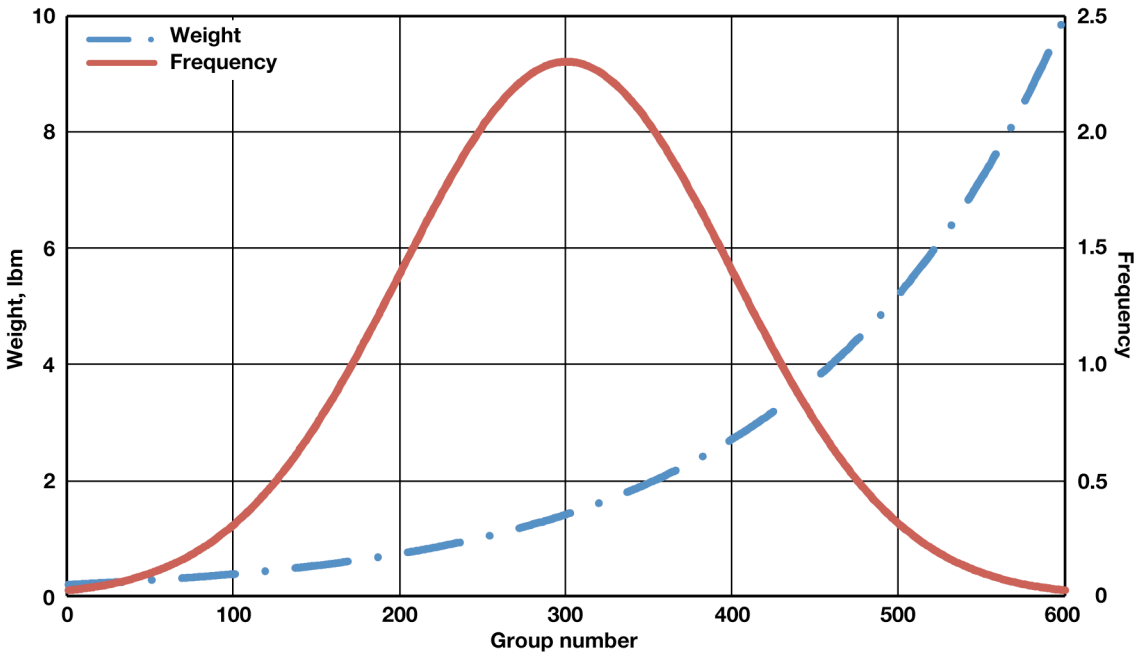

Figure 5. Weight and frequency behavior of group distribution.

A large number of weight groups, 601 in this case, were initially used to capture the behavior of the log-normal distribution. While accounting for 601 weight groups provided a comprehensive list of potential fragments, it was unnecessary to keep so many. To reduce the number of fragments provided in the catalog, the groups were discretized into larger subgroups, referred to as classes. Clustering these groups into classes provided a more manageable catalog while still capturing the desired distribution.

For this analysis, the process of generating classes from groups was done manually such that the class log-normal behavior was representative of the group behavior. For the example, the scheme shown in Table 2 is one way of clustering the group distribution into classes. The "Groups" column refers to the indices of the groups being used to create the corresponding class. The "Groups in Class, C" column refers to the number of groups being used to create the corresponding class. Using that information, the class frequencies and weights can be computed using Eqs. (5) and (6). Equation (5) provides a class frequency by summing the frequencies of the constituent groups (i.e. sum of frequencies of groups 1 through 102 for class 1). Equation (6) provides a class weight by averaging the weights of the constituent groups (i.e. average weight of groups 1 through 102 for class 1). In Eqs. (5) and (6), c is the class index, n_c is the class frequency, w_c is the class weight, y is the group index number of the first group in class c, z is the group index number of the last group in class c, and C is the number of groups in class c. The first class in the distribution shown in Table 2 has values of y equal to 1 and z equal to 102. The corresponding class frequency and weight data for the class distribution scheme in Table 2 are also shown in the table.

$$n_c = \sum_{k=y}^{z} n_k \tag{5}$$

$$w_c = \frac{\sum_{k=y}^{z} w_k}{C} \tag{6}$$

Table 2. Example of class distribution for propellant fragments.

Class	Groups	Groups in Class, C	n_c	w_c
1	1-102	102	12.840	0.283
2	103-272	170	210.200	0.710
3	273-342	70	157.600	1.488
4	343-392	50	91.750	2.192
5	393-432	40	49.540	2.934
6	433-472	40	29.480	3.808
7	473-512	40	14.980	4.943
8	513-557	45	6.958	6.526
9	558-572	15	1.065	7.911
10	573-584	12	0.590	8.638
11	585-601	17	0.556	9.497

Figure 6 shows an overlaid comparison of the group versus the class distribution. Clearly, the shape of the group distribution is not exactly preserved, and a visible offset in frequencies exists. This bias can be attributed to the manual selection of group weights that introduces user judgment in assembling the class distribution. Although this manual technique to creating classes is not ideal, it sufficiently captures the range of weights seen in the group distribution as well as the total number of fragments and total propellant weight. A more robust method of creating classes is an activity left to future studies; some ideas are presented in Section VII, "Concluding Remarks." The class distribution is the final distribution; it is an average of group clusters and can be considered an effective mean fragment of the groups that it composes.

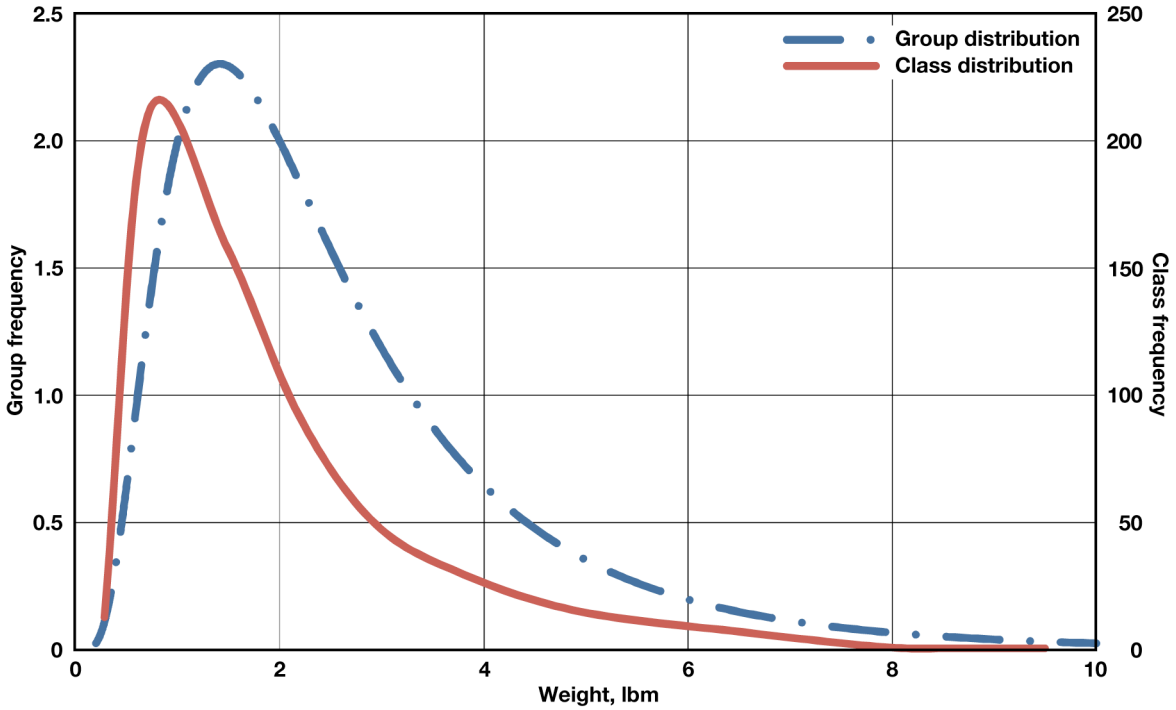

Figure 6. Group distribution compared to class distribution.

C. Ballistic Coefficient Computation

After determining fragment weights and frequency, the fragment areas were calculated assuming a generic fragment shape. For this analysis, one of two shapes was assumed: a pure cube or a cylindrical annular sector (CAS).[1] A CAS fragment, illustrated in Fig. 7, is a wedge shaped fragment of propellant created by dividing the propellant into equally sized sections. In the figure, r_1 is the outer radius of the propellant fragment, r_2 is the inner radius of the propellant fragment, and h_0 is half of the longest cross-sectional width of the propellant. Initially, a cube shaped fragment was used and the reference length (cube root of the volume) was computed for that fragment. In order to constrain the fragment dimensions, it was assumed that the longest length of a fragment could be no larger than the web thickness of the propellant.[1] If the reference length of the cube was larger than the web thickness (i.e. radial thickness) of the propellant, the fragment shape was switched to a CAS. This logic was applied for each class in the distribution created. Once a weight class had been assigned a particular shape, a reference area for that weight class was calculated based on the shape's geometry.

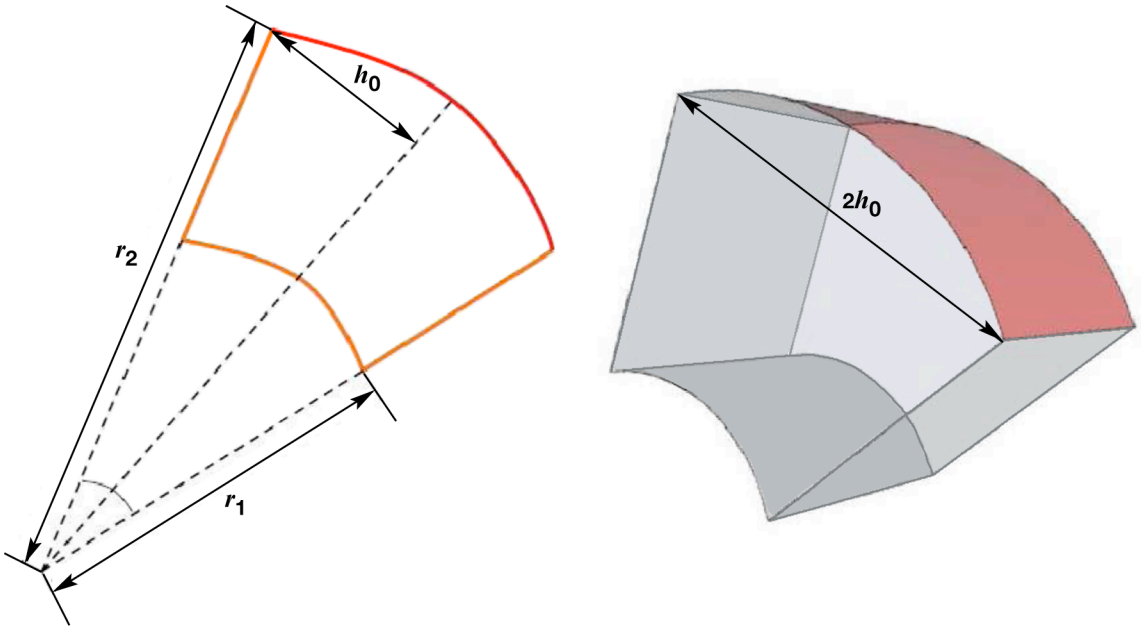

Figure 7. CAS geometry.

After area calculations were completed and added to their respective class, the first step in the debris catalog was finished, characterizing the debris distribution including fragment weight, area, shape and frequency. The information evaluated in the above analysis was then used in the computation of ballistic coefficient and imparted velocity.

The second step in completing the debris catalog was the computation of ballistic coefficients for fragments identified in the distribution. The ballistic coefficient, β, is a parameter used to describe the ability of a body to travel during flight. It can be calculated using Eq. (7) where M_{frag} is the fragment mass, S_{frag} is the fragment area, and $c_{d,frag}$ is the fragment drag coefficient.

$$\beta = \frac{M_{frag}}{c_{d,frag} S_{frag}} \tag{7}$$

This equation for ballistic coefficient expresses an inverse relationship to drag coefficient indicating that debris fragments with higher values of β will travel farther during flight. Ballistic coefficient is also increased by items with large mass to area ratios. In evaluating this expression for the PA-1 debris catalog, the mass and area terms are already computed in the assembly of the debris distribution, as described in Section IV.B, "Model Application: PA-1 Debris Catalog Distribution." Drag coefficient values are taken from previous reports outlining aerodynamic data as

a function of vehicle Mach number for propellant fragments.[1] Ballistic coefficients for each fragment class can be computed by using the distribution with this accepted aerodynamic data.

V. Fragment Ejection Velocities

The third step in this analysis is to determine the velocities imparted to the fragments released by the AM explosion. The method[6] utilized here is derived from an energy transfer approach, where a portion of the potential energy available from the overpressure is converted into kinetic energy of the fragments. This sudden release of energy generates a radial wave of pressure, which in turn applies a distribution of force across the fragments created during the blast. The force accelerates these fragments until the pressure acting on all sides of the fragments reaches equilibrium. Once this occurs, the fragments have attained an ejection velocity. This process happens quickly, usually within a few milliseconds.

An important assumption that is fundamental to this model is that the case immediately debonds from the propellant.[6] As this happens, a void or gap is left between the case and propellant that pressurizes as combustion gases exit the motor chamber. The depressurization of the chamber is essentially the pressure wave mentioned, and imparts a force on both the propellant and case fragments that are now removed from each other. Tracking the pressure change as energy travels from the chamber to the propellant-case gap (referred to as "gap" in this report) to the atmosphere provides the information necessary to determine the fragment exit velocities. Figure 8 is an illustration of the model before and immediately after the failure scenario has occurred. In Fig. 8, the three control volumes used to conduct the analysis are shown and will be explained in detail in Section V.B, "Model Propagation." Note the separation between the case and propellant (exaggerated in the figure) as well as the flow of energy and mass from the motor chamber to the atmosphere. The thermodynamic model is described in Section V.A, "Model Initialization" through Section V.E, "Final Ejection Velocity," but can be clearly summarized as such:

1) Each iteration step begins by propagating the fragment position and velocity. This is done using kinematic relationships.
2) The position change of the fragment results in new estimates for flow area and control volume.
3) The energy state of each control volume is calculated using the energy flow of the previous integration step.
4) The energy flow of the current integration step is computed using several thermodynamic relationships, mass flow, and the geometric properties found in step 2.
5) Pressure is derived from the energy state of the current iteration step and used to calculate the force acting on the fragment.
6) Force on the fragment is converted to acceleration of the fragment.
7) Fragment acceleration is used to update position and velocity in step 1. These steps are iterated until an imparted velocity is converged upon.

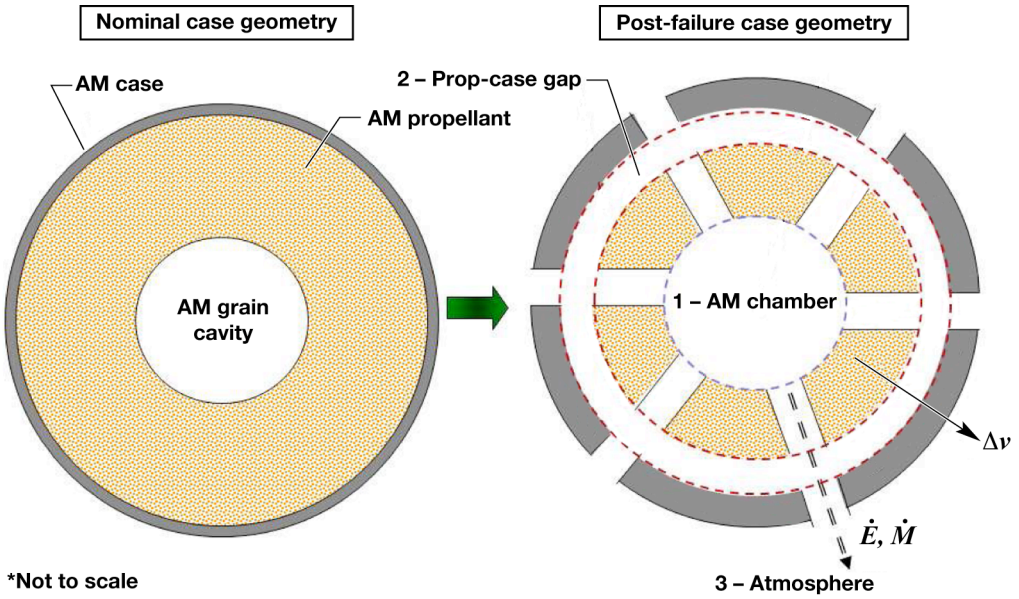

Figure 8. Illustration of the solid motor break-up model.

A. Model Initialization

The velocity model is a time based, integration model that continuously updates various parameters used to calculate velocity until the pressure in both the motor chamber and gap have reached equilibrium with the atmosphere. Several of those parameters must be initialized to a starting value, reflecting the initial state of the motor instantly after the failure occurs. First, a reference position for the propellant and case fragments, x_{frag} is set to their respective inner radii, r_{frag}. The position of the fragment is tracked as the model progresses, and is used to calculate acceleration and velocity with each integration step. Similarly, a velocity for the propellant and case fragments, v_{frag}, is initialized to zero. Because the system is being isolated, the velocities being tracked and calculated in the model are all relative to the vehicle velocity.

Pressure and energy values are also initialized based on input assumptions. The pressures of the motor chamber, P1, and the propellant-case gap, P2, are initialized to the burst pressure of the tank. Notionally, this initialization describes the events occurring at the instant of failure. The chamber has reached the burst pressure of the tank causing it to fracture, while the gap formed by the debonding of the case from the propellant immediately pressurizes to the same burst pressure. The energy of these two cavities is initialized using Eq. (8), where E is energy, P is pressure, V is volume, and γ is the ratio of specific heats of the combustion gases (it is assumed constant for the purposes of this analysis).

$$E = \frac{PV}{\gamma - 1} \tag{8}$$

B. Model Propagation

To simplify the velocity model, it is broken down into three control volumes: the motor chamber, the propellant-case gap, and the surrounding atmosphere.[6] By isolating each control volume as a segment of the model, their analyses can be done sequentially, using the outputs from one as the inputs to the next. Figure 9 is a simplified diagram of the model. Each control volume has been given a numeric designation: (1) motor chamber, (2) propellant case gap, and (3) atmosphere. This reflects the direction of flow through the entire system. Notice that, the channels through which mass and energy flow, highlighted in green, are the cracks in the propellant or case that allow the combustion products to exit the system.

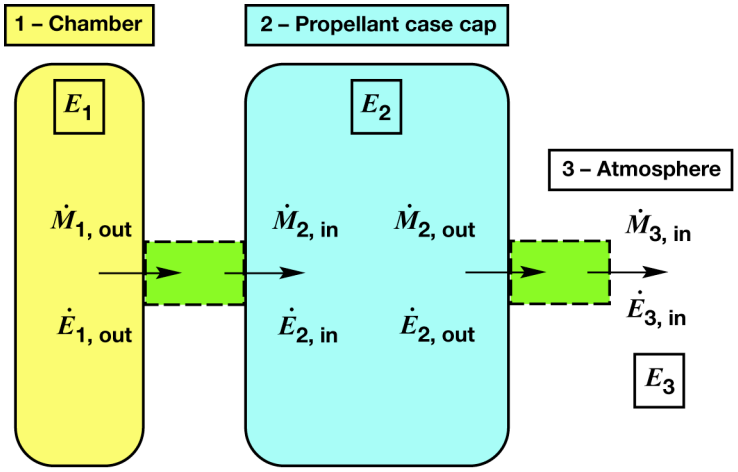

Figure 9. Illustration of the system used for energy model in ejection velocity computation.

As mentioned, this model is carried out over hundreds of time steps until a thermodynamic equilibrium has been achieved such that the chamber and gap pressures are roughly equivalent to atmospheric pressure. The time step used, on the order of microseconds, is small enough to simulate the process with fidelity sufficient to capture any high frequency dynamics. In the steps outlined below, a subscript of "i" is used to denote the current time step and a subscript of "j" is used to denote the control volume being analyzed as shown in Fig. 9. Many properties are updated using the value of the previous step denoted by the subscript "i-1." Similarly, some properties are updated using the value of a previous control volume denoted by the subscript "j-1." These calculations are performed for each

fragment class identified in Section IV.B, "Model Application: PA-1 Debris Catalog Distribution," producing ejection velocity results for each fragment in the catalog.

Each iteration of the model propagates the position and velocity of the fragment using simple kinematic relationships. Equations (9) and (10) were used to update position and velocity, where x_{frag} is the fragment position, v_{frag} is the fragment velocity, a_{frag} is the fragment acceleration, and Δt is the time step.

$$x_{frag,i} = \frac{1}{2} a_{frag,i-1} \Delta t^2 + v_{frag,i-1} \Delta t + x_{frag,i-1} \tag{9}$$

$$v_{frag,i} = a_{frag,i-1} \Delta t + v_{frag,i-1} \tag{10}$$

The surface area and volume are updated using the position of the fragment over time. As the model progresses, this control volume expands as propellant fragments move radially outward from the motor, increasing these two properties. It is important to note that surface area and volume are normalized parameters, so their values reflect a circumferential length and control area respectively. Their values can be thought of as flow area and control volume per unit length. Described in Eq. (11), surface area, *S*, refers to the flow area per unit length through which combustion gases exit the system and is used to calculate mass flow rate. Described in Eq. (12), volume, *V*, refers to the chamber volume per unit length for the first control volume, refers to the gap volume per unit length for the second control volume, and is used to calculate pressure. In these equations, *r* is the initial inner radius of the control volume, $c_{discharge}$ is the discharge coefficient of the control volume, τ_{crack} is the initial crack width in the fragment, and τ_{frag} is the fragment thickness.

$$S_{j,i} = \left(2\pi x_{fragi} - 2\pi r_j\right) c_{discharge} + \tau_{crack} \tag{11}$$

$$V_{j,i} = \pi x_{frag,i}^2 + \left(\left(2\pi x_{frag,i} - 2\pi r_j\right) + \tau_{crack}\right) \tau_{frag} \tag{12}$$

The discharge coefficient is a constant used to describe losses or inefficiencies in the flow of gas through the system. Its value can be determined either experimentally or in published data found in fluid mechanics literature.[8] For this analysis, a value of 0.72 was used based on accepted data for this type of flow model.[6]

C. Mass and Energy Balance

After propagating the fragment position, fragment velocity, and control volume geometry, the control volume energy must be updated by performing a mass and energy balance using some simple thermodynamics tools. For each time step, the energy state of the control volume is calculated followed by the energy and mass flows. The energy is calculated using the previous energy $\left(E_{j,i-1}\right)$, the previous energy flow rate $\left(\dot{E}_{j,i-1}\right)$, and the time step, Δt, as shown in Eq. (13). The energy flow rate is then calculated using an energy balance, relating energy flow rate in $\left(\dot{E}_{j,i,flow,in}\right)$, energy flow rate out $\left(\dot{E}_{j,i,flow,out}\right)$, and work rate done on the fragment $\left(\dot{W}_{i-1,frag}\right)$, as shown in Eq. (14).

$$E_{j,i} = E_{j,i-1} + \dot{E}_{j,i-1} \Delta t \tag{13}$$

$$\dot{E}_{j,i} = \dot{E}_{j,i,flow,in} - \dot{E}_{j,i,flow,out} - \dot{W}_{i-1,frag} \tag{14}$$

In Eq. (14), the work rate can be computed as shown in Eq. (15), where $F_{frag,i-1}$ is the force exerted on the fragment, and Δx is the change in fragment distance between the current and previous time steps.

$$\dot{W}_{i-1,frag} = \frac{F_{frag,i-1}\Delta x}{\Delta t} \tag{15}$$

In general, energy flow rate leaving a control volume $\left(\dot{E}_{flow,out}\right)$ is computed using mass flow and enthalpy, and is represented in Eqs. (16) to (18). In the following equations, $\dot{M}_{j,i,out}$ is the mass flow rate out of the control volume, h is the enthalpy, ρ is the density, c is the speed of sound, R is the pressure ratio between control volume j and j+1, C_v is the specific heat at constant volume, and T is the temperature.

$$\dot{E}_{j,i,flow,out} = \dot{M}_{j,i,out} h_{j,i} \tag{16}$$

$$\dot{M}_{j,i,out} = S_{j,i}\rho_{j,i}c_{j,i}\sqrt{\frac{2}{\gamma-1}\left(R_{j,i}^{\frac{2}{\gamma}} - R_{j,i}^{\frac{\gamma+1}{\gamma}}\right)} \tag{17}[6]$$

$$h_j = C_v T_{j,i} + \frac{P_{j,i}}{\rho_{j,i}} \tag{18}$$

In Eq. (18), pressure can be calculated using Eq. (8), and temperature and density can be calculated using isentropic gas laws.[9] Additionally, several boundary conditions are used to complete the energy balance of the system. For the chamber (control volume 1), it is assumed that no energy enters the system (i.e. $\dot{E}_{1,flow,in} = 0$). For the propellant-case gap, the energy flow into the system is the energy flow out of the chamber (i.e. $\dot{E}_{2,flow,in} = \dot{E}_{1,flow,out}$). Finally, for the atmospheric volume (control volume 3), the energy flow into the atmosphere is the energy flow out of the propellant-case gap, and no energy exits the final system (i.e. $\dot{E}_{3,flow,in} = \dot{E}_{2,flow,out}$ and $\dot{E}_{3,flow,out} = 0$). These assumptions are made to constrain the model and simplify the problem.

The energy flow at the current time step found in Eq. (14) is used to calculate the energy in the subsequent time step as shown in Eq. (13). With this updated energy state, the corresponding pressure can be calculated using Eq. (8). This resulting pressure is used downstream in the force and acceleration calculations.

D. Force and Acceleration Calculations

The final computation of an iteration step is that of the force and acceleration. The force is determined by the distribution of pressure across the fragment, taking the difference in pressures across its inner and outer faces. The force on each face is simply the pressure times the normalized area (the length) that the pressure acts on. Note that the computed force is actually a force per unit length. This relationship is described by Eq. (19),[6] where F_{frag} is the force per unit length acting on the fragment, and $h_{0,frag}$ is the normalized area on which the force is acting. This force is used to calculate the work done by the control volume on the corresponding fragment, shown in Eq. (15). It is also used to calculate the acceleration of the fragment, shown in Eq. (20). The mass, M_l, used in Eq. (20) is that of the fragment per unit length; in this case the reference length of the fragment. Because both force and mass are defined per unit length in this relationship, the resulting acceleration will carry standard units.

$$F_{frag,i} = 2h_0\left(P_j - P_{j+1}\right) \tag{19}$$

$$a_{frag,i} = \frac{F_{frag,i}}{M_{l,frag}} \tag{20}$$

Once the acceleration has been calculated, the time step is advanced, and the model is propagated forward. These accelerations are used in Eqs. (9) and (10) to compute position and velocity.

E. Final Ejection Velocity

While iterating to a solution, certain indicators are used to extract the final ejection velocity. Observation of pressure provides the most inherent gauge of convergence, as it directly represents the physics of the problem. As the chamber and gap depressurize, it is expected that, through the movement of energy, the pressures of the three control volumes reach equilibrium. For each simulation, the ratio of chamber pressure and gap pressure to atmospheric pressure reaches approximately one (shown in Fig. 10), meaning that the model has converged. As expected, their convergence to unity reflects the imparted velocity's approach to an ejection velocity as well as the balance of energy in the system. The system's energy state, although not shown here, is another indicator that can be used to verify the solution to ejection velocity. Using these indicators, the imparted velocity of the fragments can be determined, and the third and final step of the debris catalog is complete.

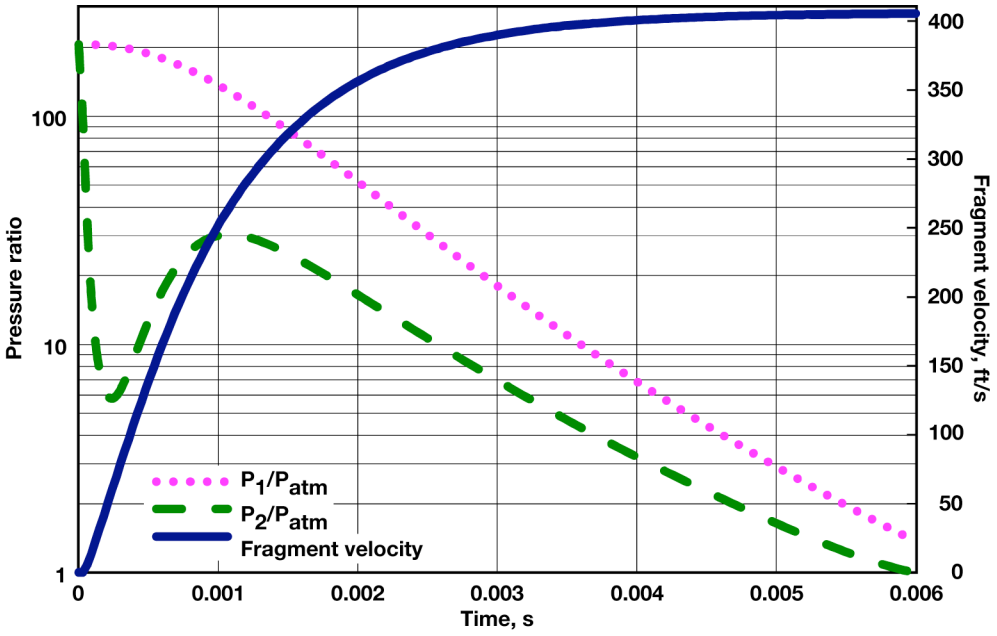

Figure 10. Indicators of final ejection velocity (0% burn stage).

VI. Results and Discussion

The methods described in Section IV, "Debris Catalog Distribution" and Section V, "Fragment Ejection Velocities" were performed at the four burn stages defined in Section III, "Debris Catalog Task Overview" to generate corresponding debris catalogs. Each catalog provides the following information for each of the eleven fragment classes derived from the log-normal distribution: weight, frequency, shape, reference area, ballistic coefficient, and imparted velocity. Table 3 is a summary of the propellant debris catalog that highlights the minimum and maximum values of reference area, weight, ballistic coefficient, and imparted velocity for each burn stage. The minimum and maximum values correspond to the smallest and largest fragment class values of weight, area, and ballistic coefficient. Conversely, the minimum and maximum values correspond to the largest and smallest fragment class values of imparted velocity results.

Table 3. Summary of debris catalog results.

	Area (in^2)		Weight (lbm)		Ballistic Coefficient (lbm/in^2)		Ejection Velocity (ft/s)	
Burn Stage	Min	Max	Min	Max	Min	Max	Min	Max
0%	3.60	162.50	0.43	41.91	50	90	403	691
25%	3.51	161.29	0.41	32.88	40	74	483	730
50%	2.89	158.49	0.31	22.99	27	32	607	789
75%	3.59	141.97	0.29	11.60	14	17	847	856

The results of this analysis do not show any unexpected behaviors, and the trends seen are consistent between burn stages. The overriding behavior seen in the data describes an inverse relationship between fragment size and fragment ejection velocity. That is, as fragment size increases, ejection velocity decreases. This behavior accounts for two trends seen in the results: (1) a decrease in velocity with increasing weight class, and (2) an increase in velocity with increasing burn stage. Weight class is a direct representation of fragment size (progressing through weight class equates to increasing fragment size), so it is clear that the first trend would also reflect an inverse relationship to ejection velocity. The second trend suggests that relative fragment size decreases through the progression of burn stages (i.e. later flight times) due to the reduced amount of propellant mass available. Figure 11 provides a plot of ejection velocity versus burn stage, confirming the second trend. Notice that, the minimum and maximum velocities almost converge by the final burn stage, indicating a tightening spread of velocities. This convergence can be attributed to the decrease in remaining propellant, which affects the range of weights seen in the weight distribution at each burn stage. This behavior can be seen in Fig. 12. With each progressive burn stage, frequencies and relative weights must see a reduction due to the decrease in available total mass.

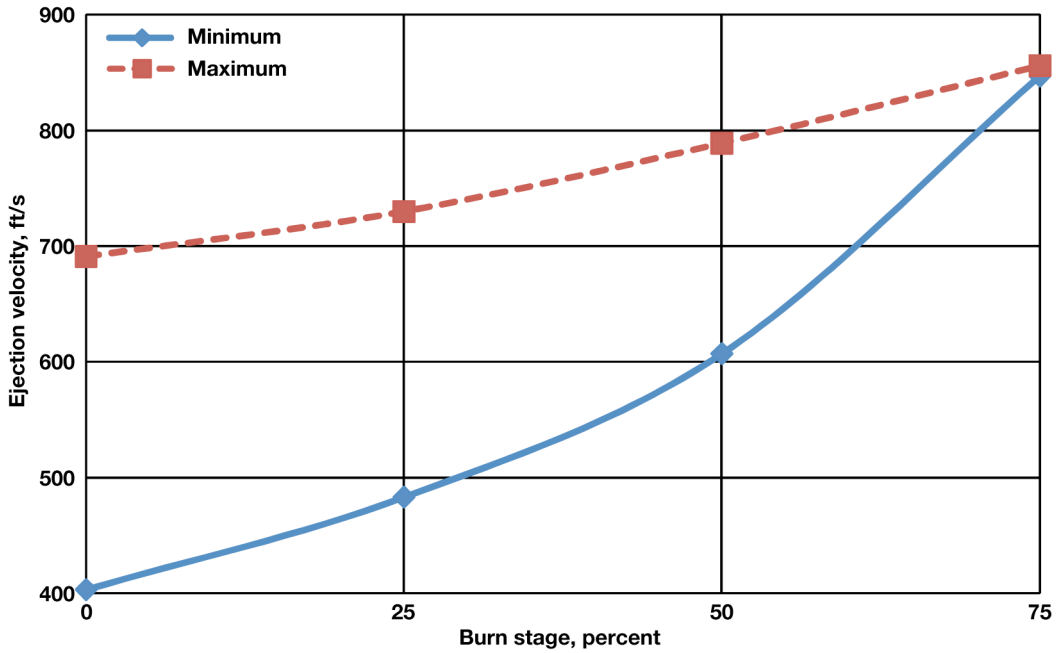

Figure 11. Ejection velocity as a function of burn stage.

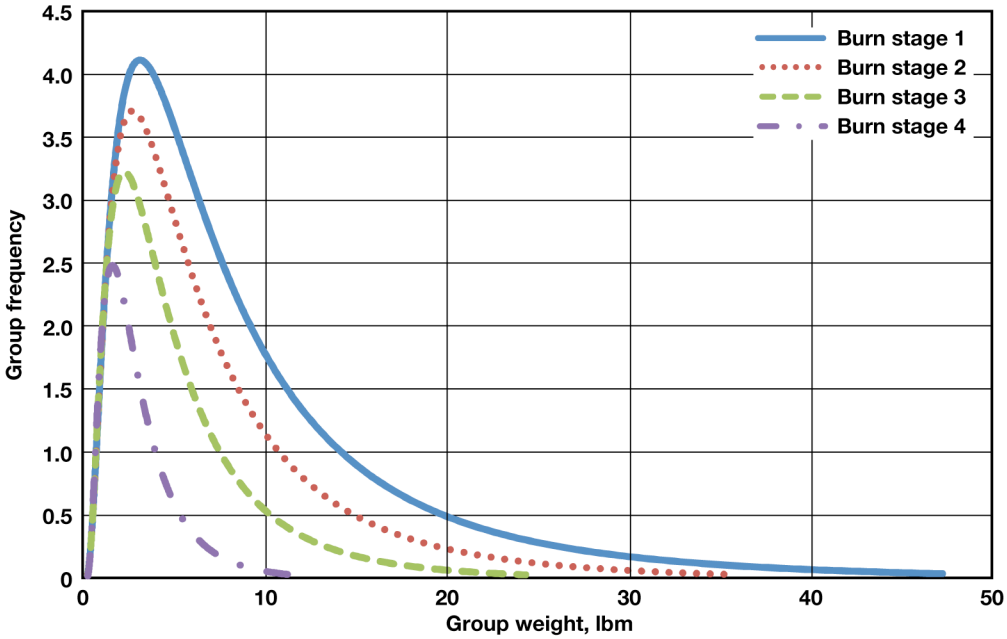

Figure 12. Comparison of group distribution.

Further investigation reveals that the relationship between fragment size and fragment ejection velocity can be attributed to the relationship between mass and area. In general, a relative increase in mass does not produce the same relative increase in area. Instead, as a fragment becomes more massive, its area increases, but not proportionally so. This relates to the velocity model in that the force being applied to smaller fragments tends to act on a larger area per unit mass than that of larger fragments. A larger force ultimately produces a larger ejection velocity, explaining how the relationship between fragment mass and area affect ejection velocity.

VII. Concluding Remarks

This report presented the debris catalog analysis performed for the Pad Abort One (PA-1) Flight Test. An overview of Orion in the context of Project Constellation was given. The Abort Flight Test (AFT) Program was described, including a summary of the PA-1 mission and vehicle configuration. A detailed description of the analysis methodology was provided. The methodology included a discussion of the debris distribution selection and application. Also included in the methodology was a description of the velocity model applied to the debris fragments to compute ejection velocities. Finally, a summary of the results was provided along with significant trends identified. The key behavior associated with the debris catalog results was determined to be the inverse relationship between propellant fragment size and fragment ejection velocity.

It is also appropriate to discuss the limitations and assumptions of the analysis as conducted here. An important limitation already mentioned is the applicability of the methods used on the Abort Motor (AM). The analysis method was taken from previous debris catalog analyses completed for much larger scale solid rocket motors such as the Space Shuttle solid rocket booster and the Titan 34D booster. For lack of better information, it was assumed that this process would be valid for the PA-1 AM. Those studies were also conducted for steel case boosters as opposed to the carbon fiber material of the AM case. It was noted previously that the AM case was not considered in the distribution analysis because of its material, and there is evidence to show that this is a valid assumption.[10] The velocity model uses the case in its analysis to define a control volume of the system; the assumption is that the composite case material can be appropriately applied to such a model. Further examination is required to understand whether these assumptions are appropriate.

For this analysis, vehicle velocity prior to destruct was used to establish drag coefficient values for fragment pieces. A more accurate approach may be to use velocity based on the vector sum of vehicle and ejection velocities. While using vehicle velocity does result in a conservative estimate of ballistic coefficient, a higher fidelity estimate should be considered.

Also mentioned previously was the manual selection of organizing weight groups into weight classes. In hindsight, a more robust approach could be used to eliminate any user bias. A future study could look at an alternate

approach, such as selecting evenly spaced weight classes and scaling the corresponding frequencies to match the shape of the group distribution and still preserve the total propellant mass. Also relegated to future studies would be an examination of using only one discretization of the distribution instead of the two as used in this method (i.e. groups and then classes).

The analysis presented for the PA-1 AM was used with the limited methods and resources that were available to the author, and while there are inherent limitations, this practice is widely accepted in the field of debris catalog analysis.

References

[1]Parker, L. C., and Ward J. A., Jr., "Solid Propellant Size Distribution Model for Large Solid Rockets," RTI Report No. RTI/5180/26-09F, 5 May, 1993.

[2]National Aeronautics and Space Administration, "Exploration Systems Architecture Study Final Report," NASA/TM-2005-214062, November 2005.

[3]Williams-Hayes, P. S., "Crew Exploration Vehicle and Launch Abort System Flight Test Overview," AIAA-2007-6596, August 2007.

[4]Idicula, J., Williams-Hayes, P., Stillwater, R., and Yates, Lt. M., "A Flight Dynamics Perspective of the Orion Pad Abort One Flight Test," AIAA-2009-5730, August 2009.

[5]Litton, D., O'Keefe, S. A., Winski, R. G. and Davidson, J. B., "Design of Launch Abort System Thrust Profile and Concept of Operations," AIAA-2008-7149, August 2009.

[6]Eck, M. B., "Shuttle Data Book SRM Fragment Velocity Model," SRB Fragment Model Review Panel, Washington D.C. 2 March, 1989.

[7]Limpert, E., Stahel, W. A. and Abbt, M., "Log-normal Distributions across the Sciences: Keys and Clues," BioScience, Vol. 51, No. 5, 2001, pp. 341-352.

[8]Ishibashi, M., and Takamoto, M., "Theoretical discharge coefficient of a critical circular-arc nozzle with laminar boundary layer and its verification by measurements using super-accurate nozzles," Flow Measurement and Instrumentation, Vol. 11, No. 4, 2000, pp. 305-313.

[9]Cengel, Y. A., and Boles, M. A., "Thermodynamics: An Engineering Approach," 4th ed., McGraw-Hill, New York, 2003.

[10]Barenberg, B., "Towpreg proves cost-competitive for wound pressure vessels," High Performance Composites, [online article], http://www.compositesworld.com/articles/towpreg-proves-cost-competitive-for-wound-pressure-vessels.aspx [cited 7 December, 2009].